Journal of Fluids and Structures (2000) **14,** 303–322
doi:10.1006/jfls.1999.0270, available online at http://www.idealibrary.com on IDEAL®

FLUID DAMPING OF AN ELASTIC CYLINDER IN A CROSS-FLOW

C. Y. Zhou and R. M. C. So

Department of Mechanical Engineering, The Hong Kong Polytechnic University Hung Hom, Kowloon, Hong Kong

and

M. P. Mignolet

Department of Mechanical and Aerospace Engineering, Arizona State University Tempe, AZ 85287, U.S.A.

(Received 11 January 1999, and in final form 5 October 1999)

Damping characteristics of fluid–structure systems are difficult to measure or calculate. In the past, such data have been rather scarce. This study reports an attempt on the use of a numerical approach to derive damping ratios related to fluid–structure interactions. It is based on an autoregressive moving-average (ARMA) method, which is used to analyse the displacement time series obtained from a numerical simulation of an elastic cylinder in a uniform cross-flow. The damping ratios show a similar trend to those obtained in previous experiments. An alternative way to deduce damping ratios is to decompose the transverse force in the structural dynamics equation into a drag (or out-of-phase) and an inertia (or in-phase) component for analysis. The damping thus deduced is in fair agreement with that obtained from ARMA; however, at or near synchronization, where the natural frequency of the stationary cylinder is close to the vortex shedding frequency, there is a very substantial difference between the two results.

1. INTRODUCTION

A fluid–structure interaction problem of common occurrence is that of a freely vibrating bluff structure in a cross-flow. The flow-induced vibrations resulting from the shed vortices can cause structural fatigue and, in certain circumstances, can lead to drastic failure of the structure. As a result, the problem has received increased attention from researchers in recent years because many modern structures use composite and lighter materials that give rise to low damping and a wide synchronization band. According to Sarpkaya (1979), synchronization occurs when the natural frequency of the fluid–cylinder system is equal to the vortex shedding frequency of the vibrating cylinder. Since this cannot be determined *a priori*, synchronization can be assumed to take place whenever the natural frequency of the cylinder is approximately equal to the vortex shedding frequency of the stationary cylinder (Zhou *et al.* 1999).

Damping models the energy dissipation during vibrations and plays an important role in the stability of the structure and its vibration amplitudes. If the dynamic behaviour of the structure were to be understood properly, one would have to have knowledge of the effects of damping. Damping may arise from the structure and from the fluid surrounding the structure. Structural damping is related to the properties of the structure itself, while fluid damping is due to viscous dissipation and fluid drag, i.e. it is the result of viscous shearing of

0889–9746/00/040303 + 20 $35.00/0

the fluid at the surface of the structure and of flow separation. Thus, fluid damping is motion-dependent and more difficult to estimate. It is generally known that the effective damping ratio ζ_e, which includes the structural damping ratio ζ_s and the fluid damping ratio ζ_f, is not constant for any structure in a flowing medium. Rather, ζ_e varies with flow velocity and vibration amplitude of the structure (Wood & Parkinson 1977). It has been shown by Griffin *et al.* (1973) that the fluid damping ratio is a function of both the structural vibration amplitude and a reduced velocity, V_r. The same result has also been found to be true in an experimental investigation carried out by Chen & Jendrzejczyk (1979), where the damping ratios in the lift and drag direction were measured. In spite of these studies, a systematic investigation of the effective and fluid damping ratios has not been carried out to-date.

There have been several mathematical models proposed to predict the vortex-induced response of a structure exposed to a cross-flow, such as the linear and nonlinear wake oscillator models (Sarpkaya 1979; Blevins 1994). These models do not include the analysis of the flow field, but couple a fluid oscillator for the fluctuating lift with a dynamic equation for the structural motion. In the course of developing these models, there arises an important question concerning the correct damping coefficient value to use in the structural dynamic equation (Skop & Balasubramanian 1997). This question has not been fully resolved even though many experimental studies have been carried out, attempting to measure the fluid damping ratio (Sarpkaya 1979).

In the past several years, a number of numerical approaches have been proposed to tackle the fully coupled fluid–structure interaction problem, where the flow field is resolved numerically. Some of these approaches are the time-marching technique proposed by Jadic *et al.* (1998), the direct numerical simulation of Newman and Karniadakis (1997) and the random walk vortex method of Slaouti & Stansby (1994). In principle, the numerical results contain most of the pertinent information relating to the flow-induced vibration problem. It is up to the investigators to extract them out for analysis. Even though these studies report in detail on the fluid–structure interaction behaviour, none has attempted to deduce damping characteristics from their results. Consequently, reliable fluid damping information on this very simple flow-induced vibration problem is still lacking.

Recently, Zhou *et al.* (1999) have carried out a rather detailed investigation of flow-induced vibrations of an elastic circular cylinder in a cross-flow. A discrete vortex method incorporating a finite difference technique was used to simulate the flow field. The cylinder response was modelled by a spring–damper–mass system while the fluid motion and the structural response were solved in a way that the interactions between the fluid and the structure were handled properly. In that study, the cylinder response, flow-induced forces, the effects of cylinder vibrations on the vortex shedding frequency and the wake vortex pattern were examined. Again, no information on fluid damping was reported.

In this paper, it is proposed to extract damping information from the results obtained by Zhou *et al.* (1999). The approach used is based on the auto-regressive moving-average (ARMA) identification technique of Mignolet & Red Horse (1994). This ARMA technique is used to analyse the time series of the structural displacements in order to deduce fluid damping ratios of the fluid–structure system. It is hoped that the information thus obtained will further enhance the understanding of the flow-induced vibrations of an elastic cylinder in a cross-flow and hence complements the work of Zhou *et al.* (1999). A secondary objective of the present study is to establish the credibility of the ARMA technique so that it can be used to deduce damping information from experimental data. In order to achieve this objective, an independent method for extracting damping information will be used to analyse the numerical data obtained by Zhou *et al.* This is the force decomposition method

where the transverse fluid force is decomposed into a drag (or out-of-phase) component and an inertia (or in-phase) component for substitution into the structural dynamics equation for analysis. The damping ratios thus deduced could substantiate those obtained from ARMA. In addition, the decomposed force components can be used to further examine the effects of the fluid motion and mass ratio on the natural frequencies of the fluid–structure system.

The use of the Zhou *et al.* (1999) data can be justified as follows. It is a numerical simulation study; therefore, all information related to displacements, pressure, forces and their respective spectra is available. This contrasts with experimental data where displacements, strain or forces are measured only. All three quantities are seldom measured together. In fact, local unsteady forces are seldom measured. Even when an attempt was made, the measurements were for situations where the structure was rigid rather than elastic (Sin & So 1987; Baban *et al.* 1989; Baban & So 1991). The ARMA technique can be used to analyse any of these signals. However, the force decomposition method requires the use of force data alone. In view of this requirement and for reasons to be discussed in the next section, the force decomposition method is limited compared to the ARMA technique. Since the force decomposition method is relatively more well-established than the ARMA technique, it could be used as an independent method to verify the ARMA deduced damping ratios away from synchronization. This is the reason why in the present study, ARMA is used to analyse the displacement signals, while the force decomposition method is applied to examine the numerically calculated unsteady forces. Thus verified, ARMA can be used with confidence to evaluate damping ratios from experimental studies where local force data is not available.

2. NUMERICAL FORMULATION

The vortex-in-cell (VIC) discrete vortex method is used to simulate the two-dimensional uniform flow past an elastic circular cylinder. For the sake of completeness, the method is briefly described below; further details can be found in Zhou *et al.* (1999). The VIC discrete vortex method represents the flow field by a number of point vortices. The motion of the fluid is then solved through tracking the evolutions of the point vortices, which includes two steps: the convection of vorticity and the diffusion of vorticity. The velocity field for the convection is obtained by solving the Poisson equation for the stream function on a mesh, while the fluid at infinity is assumed to be uniform with a velocity U_∞ in the x direction; on the surface of the cylinder, the no-slip condition is applied. The diffusion of vorticity is obtained by solving the diffusion part of the vorticity transport equation using a finite difference scheme on the same mesh.

The response of the elastic cylinder is modelled by a spring–damper–mass system. Thus the motion of the cylinder can be written as

$$m\frac{\mathrm{d}^2\boldsymbol{\chi}}{\mathrm{d}t^2} + 2m\zeta_s\omega_n\frac{\mathrm{d}\boldsymbol{\chi}}{\mathrm{d}t} + m\omega_n^2\boldsymbol{\chi} = \mathbf{F}(t), \tag{1}$$

where $\boldsymbol{\chi} = X\mathbf{i} + Y\mathbf{j}$ is the instantaneous displacement of the cylinder, $\mathbf{i}$ and $\mathbf{j}$ are unit vectors along the x and y directions, respectively, and $\mathbf{F}(t) = F_x(t)\mathbf{i} + F_y(t)\,\mathbf{j}$ is the unsteady induced force. Using D and U_∞ as the characteristic length and velocity, the dynamic equation (1) can be written in a dimensionless form as

$$\frac{\mathrm{d}^2\boldsymbol{\Psi}}{\mathrm{d}\tau^2} + 4\zeta_s\pi\mathrm{St}^*\frac{f_n^*}{f_s^*}\frac{\mathrm{d}\boldsymbol{\Psi}}{\mathrm{d}\tau} + \left(2\pi\mathrm{St}^*\frac{f_n^*}{f_s^*}\right)^2\boldsymbol{\Psi} = \frac{\mathbf{C}_f}{2M^*}. \tag{2}$$

Here, $\boldsymbol{\Psi} = \dfrac{\boldsymbol{\chi}}{D}$ and $\mathbf{C}_f = \dfrac{2\mathbf{F}(t)}{\rho D U_\infty^2}$ is the force coefficient. In this paper, an asterisk in St and f is used to denote quantities associated with the rigid (stationary) cylinder, while the same symbols without the asterisk are used to designate quantities associated with the vibrating cylinder. It should be pointed out that the parameter $\mathrm{St}^*(f_n^*/f_s^*)$ is identical to the inverse of V_r. In the present case, St* is constant because the flow Reynolds number, $\mathrm{Re} = U_\infty D/\nu$, is kept constant; therefore, only the frequency ratio varies as a result of the variation of f_n^*. This is not the case in the experimental studies of Griffin & Koopmann (1977), where U_∞ is varied instead. Therefore, in their experiments, both Re and V_r varied as a result. Equation (2) indicates that $\boldsymbol{\Psi} = \boldsymbol{\Psi}(f_n/f_s^*, \zeta_s, M^*, \mathrm{St}^*, \mathbf{C}_f)$.

In principle, the force on the cylinder is calculated by integrating the pressure and the wall shear stress on the surface of the accelerating cylinder. Zhou *et al.* (1999) used a reference frame fixed with the cylinder and superimposed a flow equal and opposite to that of the cylinder response to the flow field to account for the cylinder motion. Thus, the total force is equal to the integral around the non-accelerating cylinder, plus a force related to the acceleration of the cylinder. The response of the cylinder is determined by assuming the unsteady fluid force as the input for the right-hand side of equation (1) and solving it using the Runge–Kutta method. The flow is then solved subject to this additional flow in the next time-step. The above process of solving the fluid motion and the cylinder response is repeated in an iterative way, so that the interaction between the fluid and the cylinder can be accounted for properly.

Two approaches are used to determine the damping ratios in a fluid-structure interaction problem. These are the ARMA technique and the force decomposition method. Since the objective of the present study is to assess the relative merits of these two different approaches, it is not necessary to analyse all the cases examined by Zhou *et al.* (1999). Only selected cases with M^*, ζ_s, and f_n^*/f_s^* given by $M^* = 1$ and 10, $0{\cdot}65 < f_n^*/f_s^* < 5{\cdot}2$ and $\zeta_s = 0{\cdot}03557$, $0{\cdot}003557$ and $0{\cdot}0003557$ are used as test cases for the two approaches. The Re is set at 200 for all these cases. Therefore, they differ from the experimental cases of Griffin & Koopmann (1977), where U_∞ was varied instead. These cases have very small ζ_s; thus the effective damping ratio is essentially given by the fluid damping ratio alone and ARMA can be applied to analyse the data with relative confidence. Two cylinder vibration situations are defined. In the first situation, the cylinder is allowed to vibrate only in the transverse direction, while in the second, the cylinder is allowed to vibrate in both the x and y directions. These two situations are designated as the one-degree-of-freedom (1-dof) case and the two-degree-of-freedom (2-dof) case.

This choice of structural dynamics model, analysis techniques and Re can be justified as follows. The selection of a spring-damper-mass model to approximate the oscillation of the cylinder is based on the fact that it best represents the structural properties of the cylinder near synchronization, and the fact that, even at resonance, the cylinder does not experience very large deformation. In view of this, the choice of a linear structural model is adequate. Furthermore, near this resonance condition, the cylinder response is governed primarily (in the case of a lightly damped cylinder as is the case treated here) by the resonating mode. Thus, a one-mode approximation or equivalently a 1-dof representation of the cylinder is quite sufficient. Consequently, it is proposed to examine both the 1-dof and 2-dof cases.

The fluid–structure interaction problem under investigation is certainly not linear. Therefore, the choice of the data analysis technique requires careful scrutiny. The two choices adopted in the present study are the ARMA technique and the force decomposition technique. It is understood that the response of nonlinear systems cannot be fully described by linear models, such as ARMA. However, there are a series of properties of nonlinear systems that can be accurately captured by linear models. For example, the response of

weakly nonlinear systems is known to exhibit both a fundamental frequency and harmonics (sub- or super-) thereof. These different frequencies can be viewed as separate modes of response, each of which can be captured by the ARMA modelling technique. In this light, the ARMA technique appears to perform as a multi-frequency equivalent linearization of the fluid–structure system. Then, the very good results obtained with linear methods (Iyengar 1988) would support the use of the ARMA modelling technique for weakly nonlinear systems. On the other hand, the force decomposition method is essentially based on a one-mode, or one-frequency, representation of the cylinder vibration. Therefore, it is not appropriate in the synchronization range, where the nonlinear effects will induce both a fundamental frequency and harmonics thereof. Since the ARMA technique naturally accounts for multiple frequencies, it can best model the cylinder response time histories, even near synchronization. Consequently, the ARMA approach is expected to perform better than the force decomposition method in this range.

According to Zhou *et al.* (1999), the choice of $\mathrm{Re} = 200$ was dictated by the fact that known numerical and experimental results on a single rigid cylinder were available for comparison. This, therefore, allows the vortex dynamics method to be verified and give credence to the proposed numerical treatment of an elastic cylinder in a cross-flow. Two rigid cylinder cases at $\mathrm{Re} = 100$ and 200 have been calculated by Zhou *et al.* (1999) and the calculated Strouhal number, mean drag and root mean square fluctuating lift were found to be in very good agreement with measurements and other numerical results. These good results were obtained after a thorough study on the error and accuracy of the vortex-in-cell method and grid dependence of the numerical technique has been carried out. As for the forces, they are obtained by integrating the pressure and the wall shear stress on the surface of the cylinder. Since the pressure gradient is expressed in terms of the vorticity gradient, the force results are sensitive to the mesh size near the wall, because the calculation depends on the accuracy of the vorticity values stored in the first and second rows of the mesh. The results will converge, as the mesh size becomes finer (Zhou 1994). Tests have been conducted by Zhou *et al.* (1999) to determine the optimum mesh size. Thus, their calculations are accurate and reliable and show good agreement with other established results. Finally, it should be pointed out that even though $\mathrm{Re} = 200$ is not representative of any practical situation, it does have merits in elucidating the fundamental physics of free vibrations of a cylinder in a cross-flow. In view of these reasons, the calculations of Zhou *et al.* (1999) are credible enough for an initial attempt to extract damping information in a fluid-structure interaction problem.

3. DATA ANALYSIS

The ARMA technique is used to analyse the time series obtained from the numerical calculations. This approach considers a multi-degree-of-freedom system described by the equations of motion

$$\mathbf{M}\ddot{\mathbf{X}}(t) + \mathbf{C}\dot{\mathbf{X}}(t) + \mathbf{K}\mathbf{X}(t) = \mathbf{F}(t), \tag{3}$$

where $\mathbf{X}(t)$, $\mathbf{M}$, $\mathbf{C}$ and $\mathbf{K}$ denote the time-dependent response vector of the structure, its mass, damping and stiffness matrices, respectively, and $\mathbf{F}(t)$ represents the loading on the system. There are several steps in this approach. First, it represents the time-series data using an ARMA model, which predicts the present values as a linear combination of the past values and a white noise deviate, or

$$X_n = -\sum_{k=1}^{s} A_k X_{n-k} + \sum_{k=0}^{s-1} B_k F_{n-k} + \sum_{k=0}^{s} C_k W_{n-k}. \tag{4}$$

Here, $X_n = X(n\Delta t)$, $F_n = F(n\Delta t)$, $n = 1, 2, 3, \ldots, W_n$ is a noise vector and A_k, B_k and C_k are coefficient matrices, $k = 1, 2, 3, \ldots, s$. Introducing the notation $A_0 = I$, where I is the unit matrix, the above equation reduces to the relation

$$\sum_{k=0}^{s} A_k X_{n-k} = \sum_{k=0}^{s-1} B_k F_{n-k} + \sum_{k=0}^{s} C_k W_{n-k}. \tag{5}$$

In terms of the z transform, the above ARMA representation can be written as

$$A(z)X(z) = B(z)F(z) + C(z)W(z), \tag{6}$$

where

$$A(z) = \sum_{k=0}^{s} A_k z^{-k}, \quad B(z) = \sum_{k=0}^{s-1} B_k z^{-k}, \quad C(z) = \sum_{k=0}^{s} C_k z^{-k}, \quad X(z) = \sum_{n=-\infty}^{\infty} X_n z^{-n},$$

$$F(z) = \sum_{n=-\infty}^{\infty} F_n z^{-n}, \quad W(z) = \sum_{n=-\infty}^{\infty} W_n z^{-n}.$$

The elements of the matrices A_k, B_k and C_k are selected so that equation (4) provides a "best fit" for the computed time histories. This is mathematically achieved by maximizing the likelihood function of the observed time history (Mignolet and Red-Horse 1994). Finally, the estimates of the natural frequencies, damping ratios and mode shapes are obtained from the autoregressive part of the ARMA model. As shown in Mignolet & Red-Horse (1994), the roots, z_l, of the equation

$$\det A(z) = 0, \tag{7}$$

are related to the natural frequencies ω_l and the damping ratios ζ_l of the system by

$$\omega_l = \frac{1}{\Delta t}|\ln z_l| \quad \text{and} \quad \zeta_l = -\frac{1}{\omega_l \Delta t}\ln|z_l|. \tag{8a, b}$$

A more detailed discussion of this technique can be found in Mignolet & Red Horse (1994).

The above explanation attempts to provide the fundamental connection between vibrating structures and ARMA models. Therefore, equation (3) is representative of a general multi-degree-of-freedom system, not necessarily the fluid–structure interaction problem considered in this paper. In the current problem, however, ARMA modelling can be applied in two different ways. The first approach is to consider the cylinder alone as the structure and use the fluid forces as the excitation force, $\mathbf{F}(t)$. This modelling is certainly possible but it would yield the natural frequencies and damping ratios of the cylinder alone, i.e. in the absence of the fluid. On the other hand, the second approach is to consider both the cylinder and the fluid as the system, although only the cylinder response is observed. In this case, $\mathbf{F}(t)$ should denote the excitation external to the fluid–cylinder system, which in fact is zero in the present problem. Thus, equation (5) is used with $F_n = 0$ for all n.

In the present context of a fluid–structure interaction problem, it should be noted that the ARMA methodology yields a linear modelling of the system under consideration and thus provides a type of "equivalent linear" representation for nonlinear systems. This linearization of the system can however capture a variety of interesting features. For example, the ARMA approach generally provides a clear description of the harmonics of the fundamental frequency present in the response to which are associated "mode shapes" and

"damping ratios" which can be used to clarify the nature of these harmonics. Other versatile identification strategies, such as the Eigensystem Realization Algorithm (Juang & Pappas 1985) and the wavelet transformation (Red-Horse *et al.* 1996), also lead to linear models but are based on different mathematical properties of linear systems. When analysing the response of perfectly linear structures, these methods tend to yield natural frequencies, mode shapes, and damping ratios that are very close to each other (Red-Horse *et al.* 1996). However, in the presence of actual vibration test data, it has been found that the damping ratios are not as consistent, varying from each other by a relative margin of up to 10% (Mignolet & Red Horse 1994). It is conjectured here that these differences may be attributed to the nonlinear character of the damping mechanisms often present and to their different "linearization" performed by these methods. On this basis, it is suggested that the values of the damping ratios presented in subsequent sections should be considered as estimates. If a value of ζ is obtained, it could be expected that the true value lies in the band $[0{\cdot}9\zeta, 1{\cdot}1\zeta]$. In other words, the ζ values determined from ARMA should be attached a relative "modelling" margin of fluctuation of $\pm$ 10%.

In general, the higher the order of the model, the better the fit between the model and the original time series. However, a higher-order model will give rise to higher computational costs. Various methods have been proposed to seek an optimal order for the model (Mignolet *et al.* 1993), such as examining the values of the Akaike information criterion (AIC) and the minimum description length (MDL). In order to determine the optimal order, a group of investigations using different order are performed before the results are actually analysed. These include examining the values of AIC and MDL, and the variations of the outputs of ARMA with the model order. It is found that for most of the cases investigated, the approach with orders higher than 60 gives very consistent results. Therefore, an order 70 is chosen for all cases analysed.

The ARMA technique is capable of giving a much better frequency resolution than the fast Fourier transform (FFT) method, which is most commonly used for frequency characteristics identification. This is important, especially when the damping ratio of the fluid–structure system is small and the transfer frequency function shows a sharp peak around the vortex shedding frequency. The ARMA technique has been used by So *et al.* (1999) to determine the damping ratios and mode shapes of an elastic thin aerofoil in flight. Such information is very difficult to obtain from the simple FFT method.

4. DAMPING FROM ARMA ANALYSIS

Since the vibration in the y direction is much more pronounced compared to that in the x direction, as a first attempt, fluid–structure damping is extracted from the time series of the y displacements in the 2-dof computations. The cylinder displacements (Zhou *et al.* 1998) for the test cases specified above are analysed using the ARMA approach. The results of the effective damping ratio given by $\zeta_e = \zeta_s + \zeta_f$ are plotted versus the frequency ratio f_n^*/f_s^*. For the different cases examined, the results show a similar trend (Figures 1–4), i.e. when f_n^*/f_s^* decreases from 5.2 to 0.65, ζ_e decreases slightly first and then experiences a valley at $f_n^*/f_s^* \sim 1$. This is followed by a very sharp increase to a relatively high value when $f_n^*/f_s^* < 1$.

An attempt is first made to compare this calculated trend with the experimental trend measured by Griffin & Koopmann (1977), where the velocity of the oncoming flow was varied to produce different frequency ratios rather than changing f_n^* as in the calculations of Zhou *et al.* (1999). Their results, therefore, included the effects of the variations of V_r and Re, while in the numerical calculations of Zhou *et al.* (1999) only the effects of the variation of f_n^* were examined. In view of this difference, a direct comparison of these results is not very

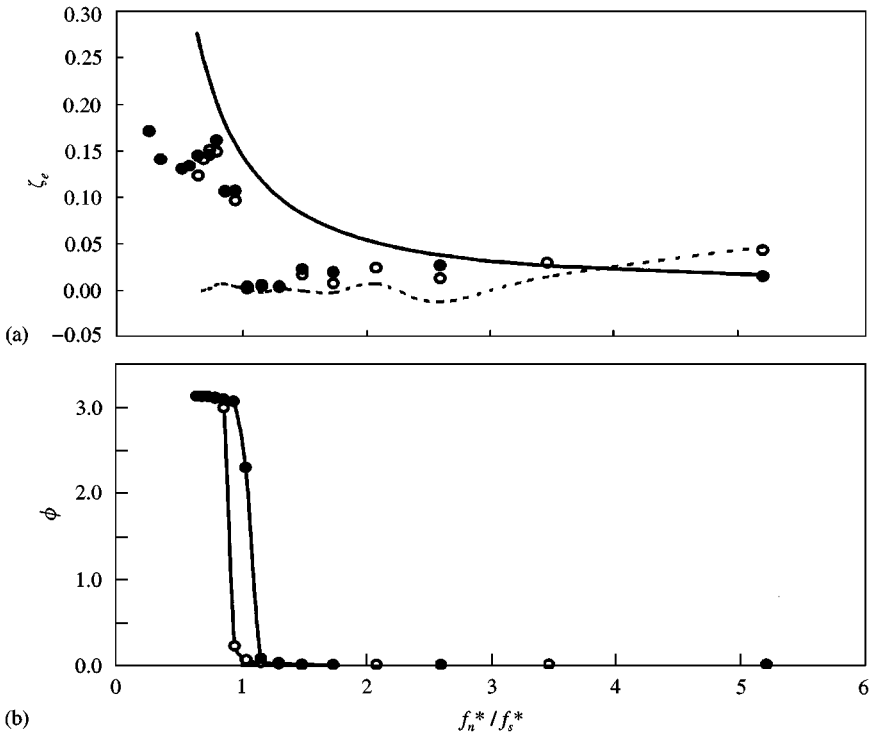

Figure 1. (a) Variation of ζ_e with f_n^*/f_s^*: ○, $M^* = 1$, $\zeta_s = 0{\cdot}003557$, 2-dof; ●, $M^* = 1$, $\zeta_s = 0{\cdot}003557$, 1-dof; ——, equation (15), $M^* = 1$; ---, equations (14) & (16), $M^* = 1$. (b) Variation of ϕ with f_n^*/f_s^*: —○—, $M^* = 1$, $\zeta_s = 0{\cdot}003557$, 2-dof; —●—, $M^* = 1$, $\zeta_s = 0{\cdot}003557$, 1-dof.

appropriate. Even then, a qualitative comparison could be made. Griffin and Koopmann (1977) observed that the fluid damping changes slowly at low flow velocity and then decreases to a minimum as the velocity increases to within the synchronization range. Furthermore, the minimum range of damping occurs near the maximum amplitude of the cross-flow vibrations. As the synchronization range is crossed, the damping increases more rapidly with flow velocity. This behaviour is very similar to that shown in Figures 1–4.

A second comparison is made between a 1-dof and a 2-dof case for the same M^* and ζ_s [Figure 1(a)]. It can be seen that the ζ_e behaviour for the two cases is very similar. One difference is that the sharp increase in ζ_e occurs at a lower value of f_n^*/f_s^* for the 2-dof case than for the 1-dof case. This trend agrees with the behavior of the vortex patterns, force coefficients and displacement amplitudes of the two cases examined by Zhou *et al.* (1999), i.e., the same physical phenomenon always lags behind in the 2-dof case as the value of f_n^*/f_s^* varies from 5·2 to 0·65. The sharp increase in ζ_e is caused by a rapid change in the phase angle ϕ between the lift force and the cylinder displacement [Figure 1(b)]. This result is remarkably consistent with the phase plot of a lightly damped single-degree-of-freedom vibrating system which undergoes a rapid transition from 0 to π as resonance is crossed. At or near synchronization, i.e. $f_n^*/f_s^* \sim 1$, the damping ratio of the system experiences a valley. This implies low-energy dissipation and high-energy transfer from the flow to the cylinder during the synchronization process. Further evidence in support of this interpretation can be gleaned from an analysis of the behaviour of the lift drag coefficient after the unsteady lift force has been decomposed into an inertia component and a drag component. The latter

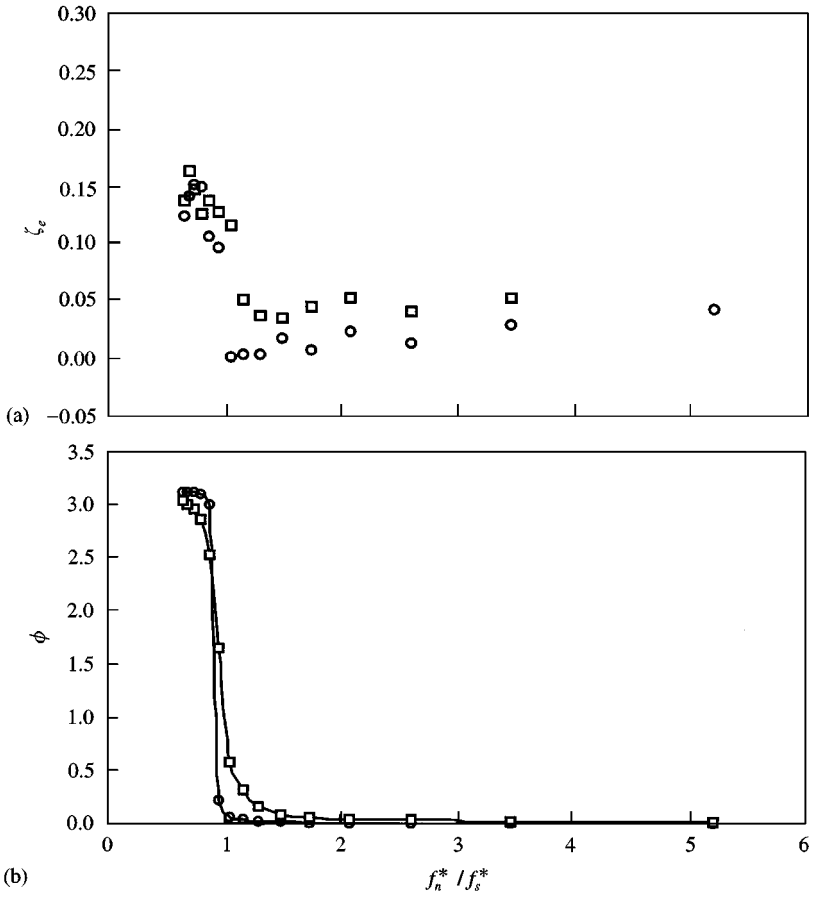

Figure 2. (a) Variation of ζ_e: ○, $M^* = 1$, $\zeta_s = 0{\cdot}003557$, 2-dof; □, $M^* = 1$, $\zeta_s = 0{\cdot}03557$, 2-dof. (b) Variation of ϕ with f_n^*/f_s^* for two different values of ζ_s: —●—, $M^* = 1$, $\zeta_s = 0{\cdot}003557$, 2-dof; —□—, $M^* = 1$, $\zeta_s = 0{\cdot}03557$, 2-dof.

component is called a lift drag component and the coefficient a lift drag coefficient. A detailed discussion of this is given in the next section.

The third comparison is made between two cases with the same M^* but different ζ_s [Figure 2(a)]. It can be seen that there is very little difference in ζ_e between the two cases, because the difference in ζ_s is quite small compared to ζ_f. However, the phase angle ϕ shows a smoother change for the case with a higher structural damping ratio, i.e. $\zeta_s = 0{\cdot}03557$ [Figure 2(b)], a result which is again completely consistent with a single-degree-of-freedom oscillator properties. It should be noted that the damping ratio corresponding to $f_n^*/f_s^* = 5{\cdot}2$ and $\zeta_s = 0{\cdot}03557$ is not presented in Figure 2(a) because of the lack of reliability of its estimate obtained by the ARMA modelling method for which this configuration is the most challenging one. Indeed, all natural frequencies and damping ratios are extracted by the ARMA approach from the transient response of the cylinder which occurs from $t = 0$ until the system settles, exhibiting only the harmonics of the shedding mechanism. Following standard vibration arguments, this settling time is approximately inversely proportional to both the total damping ratio and the actual natural frequency of the system and thus is the smallest when $f_n^*/f_s^* = 5{\cdot}2$ and $\zeta_s = 0{\cdot}03557$. This configuration is thus characterized by an extreme shortness of the transient phase, which hinders the reliable identification of the low-energy free response within the displacement time series.

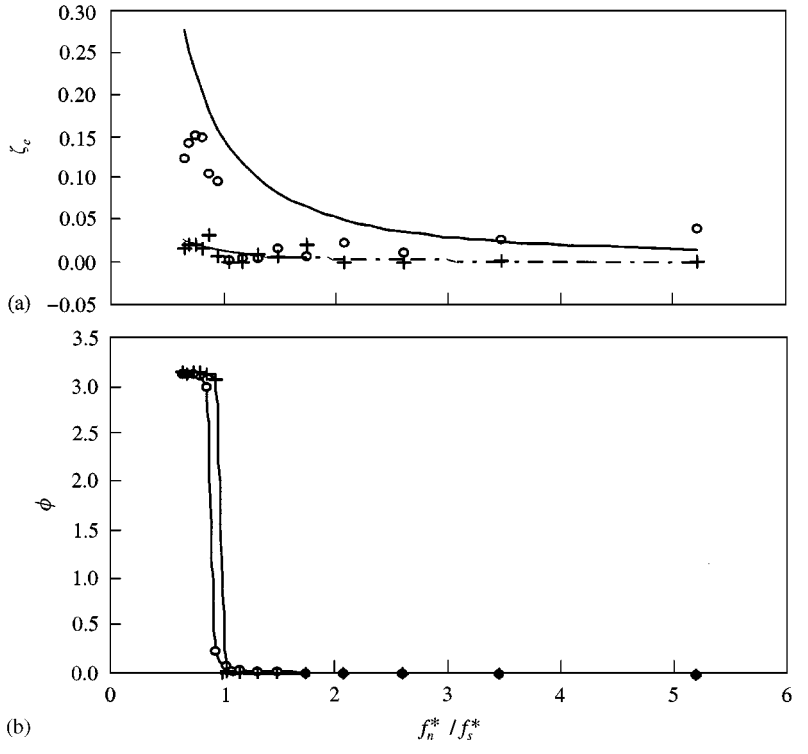

Figure 3. (a) Variation of ζ_e: ○, $M^* = 1$, $\zeta_s = 0{\cdot}003557$, 2-dof; +, $M^* = 10$, $\zeta_s = 0{\cdot}0003557$, 2-dof; ——, equation (15), $M^* = 1$; – – . ., equation (15), $M^* = 10$. (b) Variation of ϕ with f_n^*/f_s^* for two different values of M^* and ζ_s: —○—, $M^* = 1$, $\zeta_s = 0{\cdot}003557$, 2-dof; —|—, $M^* = 10$, $\zeta_s = 0{\cdot}0003557$,, 2-dof.

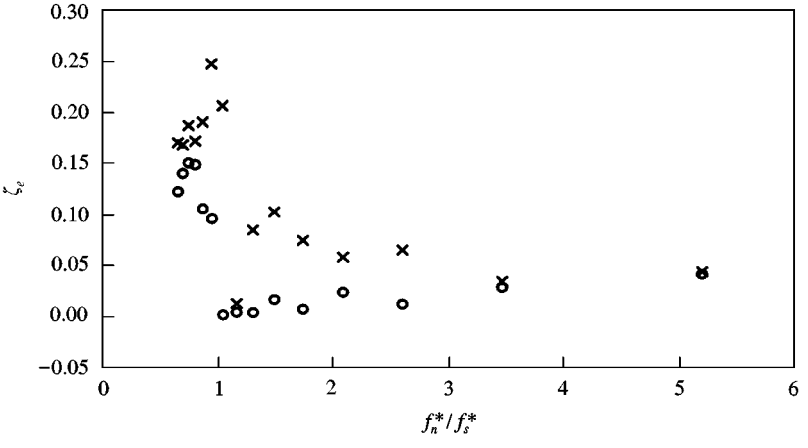

Figure 4. Comparison of ζ_e determined from the X and Y displacements: ×, x-direction, $M^* = 1$, $\zeta_s = 0{\cdot}003557$; ○, y-direction, $M^* = 1$, $\zeta_s = 0{\cdot}003557$.

Finally, the last comparison is made between two cases with different M^* and different ζ_s [Figure 3(a)]. The results show that the value of ζ_e for the $M^* = 10$ case is much smaller than that for the $M^* = 1$ case at or near synchronization. This behaviour is consistent with expectation, i.e. the larger the mass ratio the smaller the damping ratio. The ϕ plot

[Figure 3(b)] shows a very sharp jump for both cases though. However, the jump occurs at a lower value of f_n^*/f_s^* in the $M^* = 10$ case compared to the $M^* = 1$ case. This observation appears to be quite physical since, as M^* is increased, the effect of the fluid on the structure is decreased. Further, besides damping the cylinder vibrations, the fluid primarily provides an added mass effect to the structural system. Then, the natural frequency of the fluid-structure system will stay higher for $M^* = 10$ than for $M^* = 1$ and a lower value of f_n^*/f_s^* will be required to have resonance with the almost constant shedding frequency for $M^* = 10$ than for $M^* = 1$.

Since fluid damping is motion dependent, there is no reason to expect it to be the same in both the x and y directions. The present results provide further evidence to support this interpretation. Figure 4 shows the comparison between the damping ratio in the x direction, ζ_{ex}, and that in the y direction, ζ_{ey}. It is seen that the value of ζ_{ex} is larger than that of ζ_{ey} at or near synchronization. This shows that the vibration in the y direction is even more dominant when synchronization occurs. It is also noticed that the location where ζ_{ex} reaches a minimum ($f_n^*/f_s^* = 1{\cdot}2$) is different from $f_n^*/f_s^* \sim 1$, where ζ_{ey} has its lowest value. The fact that the damping ratio ζ_{ex} is larger than ζ_{ey} has been previously shown by Blevins (1994), who used simple deduction and certain linear approximations to deduce ζ_{fx} and ζ_{fy}, which are given by

$$\zeta_{fx} = \frac{1}{4\pi}\frac{U_\infty}{f_n D}\frac{1}{M^*}C_D, \quad \zeta_{fy} = \frac{1}{8\pi}\frac{U_\infty}{f_n D}\frac{1}{M^*}C_D. \tag{9}$$

It is obvious that $\zeta_{fx} > \zeta_{fy}$. Therefore, it also follows that ζ_{ex} is larger than ζ_{ey}. The same conclusion can also be drawn from the experimental investigation of Chen and Jendrzejczyk (1979).

5. DAMPING FROM UNSTEADY FORCE DECOMPOSITION

An alternative way to extract damping information is to attempt to decompose the excitation force in the transverse direction into a drag or out-of-phase component and an inertia or in-phase-component for substitution into equation (1) for analysis (Sarpkaya 1981). This analysis, therefore, ignores the coupling between the x and y directions and assumes that the fluid damping is derived mainly from the oscillations in the y direction. Since vortex shedding is more or less a sinusoidal process, it is reasonable to assume that the transverse force acting on the cylinder undergoes harmonic variations. Therefore, the displacement of the cylinder in the y direction may be assumed to be approximated by $Y(t) = Y_{\max}\sin(\omega_s t)$, while the instantaneous velocity and acceleration can be determined as $V(t) = V_{\max}\cos(\omega_s t)$ and $a_y(t) = -\omega_s V_{\max}\sin(\omega_s t)$, respectively. The transverse force $F_y(t)$ leads the excitation by a certain phase angle and may be decomposed into a drag term and an inertia term which can be called "lift drag force" and "lift inertia force" since both are in the lift direction. Thus decomposed, the transverse force can be written as

$$F_y(t) = -\frac{1}{2}\rho D V_{\max}^2 C_{dl}|\cos(\omega_s t)|\cos(\omega_s t) - \frac{\pi D^2}{4}\rho C_{ml} a_y(t). \tag{10}$$

It is known that for a cylinder vibrating with small amplitude in a stationary fluid, the inertia coefficient C_{ml} is equal to the added mass coefficient C_a with a value around 1 for a circular cylinder. For a stationary circular cylinder in a small-amplitude oscillatory flow, $C_{ml} = 1 + C_a \approx 2$, which can be interpreted as the sum of a pressure force (resulting from the mean pressure gradient in the fluid) and an added mass force. In general, the added mass coefficient is not exactly 1 ($C_a \neq 1$). Its value will depend on the type of motion of the body

and/or the fluid motion around the body. In the present situation, C_{ml} represents the sum of both the added mass force and the fluid lift force in the direction of the cylinder acceleration. Nondimensionalizing equation (10) by using $\frac{1}{2}\rho D U_\infty^2$ and rearranging gives

$$\frac{F_y(t)}{\frac{1}{2}\rho D U_\infty^2} = -C_{dl}\left(\frac{V_{\max}}{U_\infty}\right)^2 |\cos(\omega_s t)|\cos(\omega_s t) + C_{ml}\pi^2 \,\mathrm{St}\frac{V_{\max}}{U_\infty}\sin(\omega_s t). \tag{11}$$

If the term $\cos(\omega_s t)|\cos(\omega_s t)|$ is expanded in series and only the first term is retained, equation (11) becomes

$$\frac{F_y(t)}{\frac{1}{2}\rho D U_\infty^2} = -C_{dl}\frac{8}{3\pi}\left(\frac{V_{\max}}{U_\infty}\right)^2 \cos(\omega_s t) + C_{ml}\pi^2 \,\mathrm{St}\frac{V_{\max}}{U_\infty}\sin(\omega_s t). \tag{12}$$

Substituting equation (12) into the y component of equation (1), the equation governing the displacement in the y direction can be written as

$$m\frac{\mathrm{d}^2 Y}{\mathrm{d}t^2} + 2m\omega_n\left(\zeta_s + \frac{2}{3\pi}\frac{1}{M^*}\frac{f_s}{f_n}\frac{Y_{\max}}{D}C_{dl}\right)\frac{\mathrm{d}Y}{\mathrm{d}t} + m\omega_n^2 Y = C_{ml}\pi^2 \,\mathrm{St}\frac{V_{\max}}{U_\infty}\sin(\omega_s t), \tag{13}$$

and the fluid damping ratio ζ_f is given by

$$\zeta_f = \frac{2}{3\pi}\frac{1}{M^*}\frac{f_s}{f_n}\frac{Y_{\max}}{D}C_{dl}. \tag{14}$$

This formula indicates that ζ_f is directly proportional to Y_{max}/D and the frequency ratio f_n/f_s. However, it is inversely proportional to the mass ratio M^*. Since the lift drag coefficient C_{dl} is also a function of these parameters, the relation between ζ_f, $Y_{\max}/D$ and M^* may not be as simple as equation (14) indicates. When synchronization occurs, nonlinearity becomes more and more important. As a result, the relationship between fluid damping and these parameters will become even more complicated. In spite of these concerns and to the lowest order, relation (14) could be used to assess the dependence of the fluid-damping ratio on these parameters, especially when experimental data are not available.

If the analogy is drawn between the present vibrating cylinder case and that of a two-dimensional cylinder in small-amplitude oscillation without separation, then the drag coefficient C_{dl} in equation (14) could be deduced from the solution given by Stokes for the small-amplitude oscillation problem. Noting that over a cycle of oscillation $\cos(2\pi f)|\cos(2\pi f)|$ could be approximated by $(8/3\pi)\cos(2\pi f)$, the first term of its Fourier expansion series, the Stokes' solution for the drag coefficient (Batchelor 1970) is then given by $C_d = (3\pi^2/4)(D/Y_{\max})\sqrt{\nu/\pi f D^2}$. Taking this solution of C_d as C_{dl} in equation (14), assuming f to be given by f_n and substituting into equation (14) gives

$$\zeta_f = \frac{\sqrt{\pi}}{2}\frac{1}{\mathrm{M}^*}\frac{f_s}{f_n}\sqrt{\frac{V_{rs}}{\mathrm{Re}_s}}, \tag{15}$$

where $V_{rs} = V_{\max}/f_n D$ and $\mathrm{Re}_s = V_{\max} D/\nu$ are defined for convenience. By analogy, Re_s can be taken to be the same as Re, and V_{rs} to be given by $U_\infty/f_n D$. Results thus calculated are plotted in Figure 1(a) for the case where $M^* = 1$ and $\zeta_s = 0{\cdot}003557$ and in Figure 3(a) for the two cases where $M^* = 1$, $\zeta_s = 0{\cdot}003557$ and $M^* = 10$, $\zeta_s = 0{\cdot}0003557$.

A close agreement between equation (15) and the damping ratio results deduced from ARMA cannot be expected since, in the present situation, the flow is always separated and, furthermore, when synchronization occurs, the amplitude of the vibration becomes quite

large ($\sim 0{\cdot}5D$). However, it is instructive to plot equation (15) for comparison because it could shed light on the functional dependence of ζ_f on parameters such as M^* and f_n^*/f_s^*. It can be seen from Figure 1(a) and 3(a) that this simple relation (15) does show a similar trend as the ARMA results in terms of the parameters f_n^*/f_s^* and M^*; i.e. as f_n^*/f_s^* decreases, ζ_f increases, and when M^* increases, ζ_f decreases. When the frequency ratio is much larger than 1 and the amplitude of the vibration is small, the ARMA results are quite close to those deduced from equation (15). However, as expected, large differences appear in the region surrounding synchronization. Here, the ARMA deduced damping ratios are much smaller than the predictions of equation (15). There are numerous reasons for the discrepancy; chief among them are the inappropriateness of equation (15), since the Stokes formula for the drag is for attached flow only, and the inability of the force decomposition method to model the nonlinear character of the fluid–structure interactions near synchronization. Therefore, for reasons explained above, the ARMA results near synchronization are expected to be more reliable than those deduced from the force decomposition method.

The fluid damping ratio could further be determined from equation (14), but with the drag coefficient C_{dl} evaluated from the time history of the transverse fluid force in the following way. In general, the force coefficients C_{dl} and C_{ml} in equation (12) are functions of time; however, their averages can be evaluated as

$$C_{dl} = -\frac{3}{4}\int_0^{2\pi} \frac{F_y(t)\cos(\omega_s t)}{\rho V_{\max}^2 D}\,\mathrm{d}(\omega_s t), \tag{16a}$$

$$C_{ml} = \frac{2V_{\max}}{\pi^3 f_s D}\int_0^{2\pi} \frac{F_y(t)\sin(\omega_s t)}{\rho V_{\max}^2 D}\,\mathrm{d}(\omega_s t). \tag{16b}$$

Before examining the result of equations (14) with (16) substituted for C_{dl}, the behaviour of the force coefficients are examined first. The results of C_{dl} and C_{ml} thus obtained from equation (16) by numerically integrating the above expressions with the time series $F_y(t)$ are presented in Figure 5(a) and Figure 5(b), respectively, for the 1-dof and 2-dof cases. It is seen that, when f_n^*/f_s^* is much larger than 1 and the vibration amplitude is very small, C_{ml} approaches unity while C_{dl} becomes relatively large. The values of the lift inertia and lift drag coefficients in this range of f_n^*/f_s^* are very close to those for a cylinder undergoing small-amplitude oscillations in a quiescent fluid. As f_n^*/f_s^* approaches 1 and the vibration amplitude increases, C_{dl} drops rapidly while C_{ml} increases slightly first and then reaches a maximum of about 2 just before synchronization occurs. Thereafter, it decreases sharply below 1 and reaches a minimum at $f_n^*/f_s^* \sim 1$. The rapid drop in C_{ml} occurs when the fluid–structure system undergoes synchronization. For $f_n^*/f_s^* < 1{\cdot}0$, both C_{dl} and C_{ml} are seen to have relatively steady values. The result of the lift inertia coefficient analysis, therefore, indicates that using the added mass coefficient $C_a = 1$ to model the vortex-induced vibration is not quite proper. The natural frequency of the fluid–structure system assuming $C_a = 1$ may be underestimated when f_n^*/f_s^* is in or falls below the synchronization range. This phenomenon will be further discussed in the next section.

For the 1-dof and 2-dof cases, the variation of C_{dl} and C_{ml} with f_n^*/f_s^* are quite similar. However, the value of C_{dl} for the 2-dof case appears to be slightly larger than that for the 1-dof case, while the opposite is true for C_{ml}. The reason for this is not known at present. It could be due to the fact that restricting the cylinder vibration to just one direction could have an undue effect on the behaviour of these parameters. In other words, the coupling between the vibrations in the x and y directions cannot be ignored, even for this rather simple case of an elastic cylinder in a cross-flow.

Previously, equation (10) was normalized by using the term $\frac{1}{2}\rho D U_\infty^2$ and the result was equation (11). However, the term $\frac{1}{2}\rho D V_{\max}^2$ may be more sensitive to the motion in the

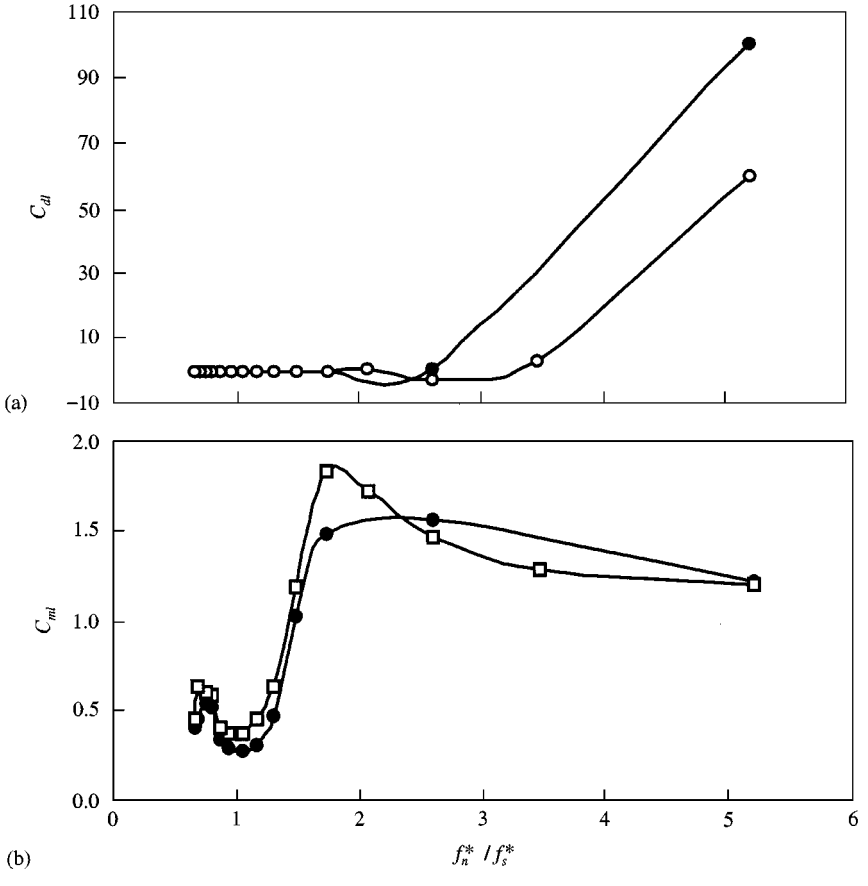

Figure 5. (a) Variation of C_{dl} with f_n^*/f_s^*: —●—, 1-dof; —○—, 2-dof. (b) Variation of C_{ml} with f_n^*/f_s^*: —●—, 1-dof; —□—, 2-dof.

y direction than the term $\frac{1}{2}\rho DU_\infty^2$. Therefore, it is suggested to re-examine the force behaviour by normalizing the transverse fluid force (10) using the term $\frac{1}{2}\rho DV_{\max}^2$. The result is

$$\frac{F_y}{\frac{1}{2}\rho DV_{\max}^2} = -C'_{dl}\cos(\omega_s t) + C'_{ml}\sin(\omega_s t), \tag{17}$$

where C'_{dl} and C'_{ml} are related to C_{dl} and C_{ml} by the following relations:

$$C'_{dl} = \frac{32\pi}{3}\left(\frac{Y_{\max}}{D}\right)^2 \mathrm{St}^2\, C_{dl}, \tag{18a}$$

$$C'_{ml} = 2\pi^3 \frac{Y_{\max}}{D}\mathrm{St}^2\, C_{ml}. \tag{18b}$$

The variations of C'_{dl} and C'_{ml} with f_n^*/f_s^* are plotted in Figure 6. It can be seen that the lift drag coefficient becomes negative at $f_n^*/f_s^* \sim 1{\cdot}0$, which is more visible in Figure 6(a). This negative behaviour indicates that the lift drag force is in phase with the velocity of the cylinder and helps to magnify the vibrations rather than damp them out. It also suggests

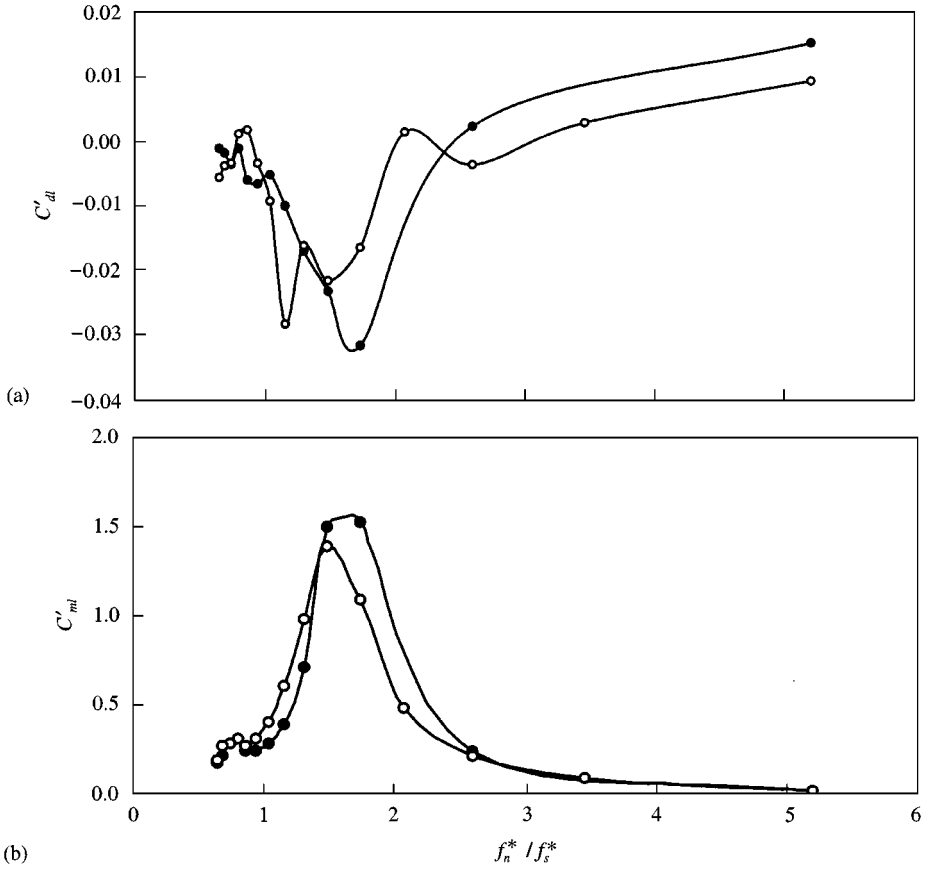

Figure 6. (a) Variation of C'_{dl} with f_n^*/f_s^*: —●—, 1-dof; —○—, 2-dof. (b) Variation of C'_{ml} with f_n^*/f_s^*: —●—, 1-dof; —○—, 2-dof.

that the direction of energy transfer is from the fluid to the cylinder and this is accomplished through the mechanism of synchronization.

Once the transverse force is known, C_{dl} can be determined from equation (16) and ζ_f from equation (14). The result is plotted in Figure 1 as the dashed curve. It is seen that the curve is in reasonable agreement with the results obtained from ARMA in the range of $f_n^*/f_s^* > 1$ but a substantial discrepancy appears in the range of $f_n^*/f_s^* < 1$. The poor agreement could be due to a number of reasons. Certainly, a major one is the importance of nonlinear interaction at or near synchronization; therefore, both the ARMA method and the force decomposition technique which are based on linear assumptions may not represent the situation completely. Another reason could lie in the value assumed for C_{dl}. The value of C_{dl} in fact represents the total force component as it is derived in the direction of the cylinder velocity in the y direction, i.e. $V(t)$. According to Griffin and Koopmann (1977), this component should include the components of excitation force which is in-phase with $V(t)$ and the fluid reaction force, or the fluid damping, which is in-phase but is opposite to that of $V(t)$. In other words, the damping force is only part of it. Furthermore, it has been found from the lift force time histories that, in the range of $f_n^*/f_s^* < 1$, a lower frequency related to the natural frequency of the cylinder settles in. The assumption of simple harmonics for the shedding frequency cannot represent the lift force properly, even to the lowest order. The agreement in the range $f_n^*/f_s^* > 1$ suggests that the main part of the drag force is the

damping force, hence the lift force decomposition, as proposed in equation (16), could be appropriate in that frequency range.

6. M* EFFECT ON THE SYSTEM NATURAL FREQUENCY

The natural frequency f_n of the fluid–structure system may be estimated from the stiffness and the effective mass of the system, which includes the structural mass and the added mass due to fluid motion. When the mass ratio between the structure and the fluid is small, the effect of the added mass on f_n is important since it influences the frequency ratio range at which synchronization occurs. Generally, the smaller the mass ratio, the wider is the range of frequencies f_n^*/f_s^* corresponding to the vibration peak band. To investigate this effect, a relation between f_n and f_n^* has been derived by Zhou *et al.* (1999) assuming $C_{ml} = C_a = 1$. The relation was obtained by moving the added mass term from the right-hand side to the left-hand side of equation (10) to form the effective mass of the system. The relation in its more general form is given by

$$f_n = f_n^*/\sqrt{1 + C_a(4/\pi M^*)}. \tag{19}$$

The results of f_n determined from ARMA for the different cases are presented in Figures 7–9 together with the results deduced from equation (19) for the $M^* = 1$ and 10 case. When f_n^*/f_s^* is much larger than 1 and $\zeta_s = 0{\cdot}003557$, equation (19) appears to give a fairly good estimate of f_n, as can be seen from Figure 7. For higher values of ζ_s, such as $\zeta_s = 0{\cdot}0357$ (Figure 8), the agreement between the ARMA results and equation (19) is not as good as for the case where $\zeta_s = 0{\cdot}003557$. When f_n^* is approximately equal to f_s^*, the comparison indicates that f_n does not follow the relation given by equation (19). Instead, it is consistently higher than that given by equation (19). This is clearly shown in Figure 9. The underestimation of equation (19) is due to the fact that C_{ml} drops below 1 as synchronization occurs. This is evident from equation (19) because when C_a is less than 1, $f_n = f_n^*/\sqrt{1 + C_a(4/\pi M^*)} >$

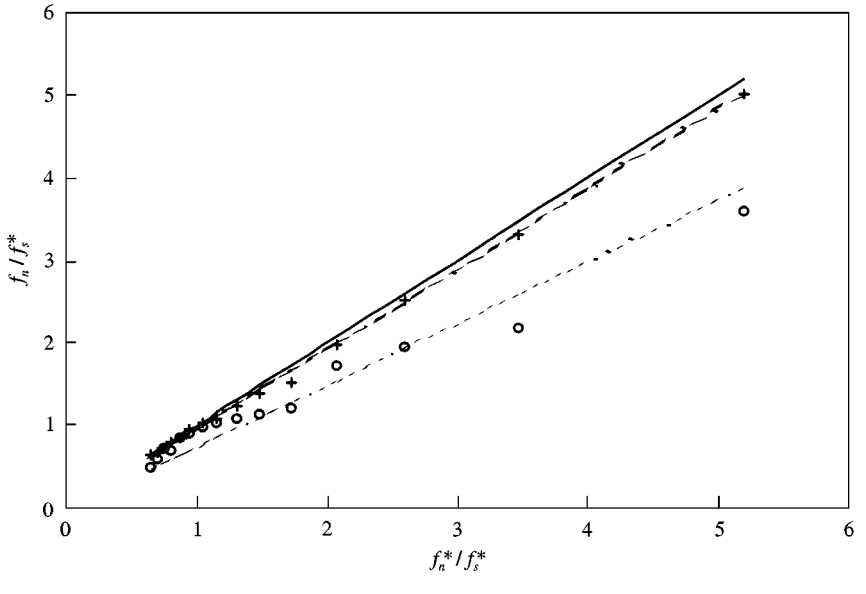

Figure 7. Variation of f_n with f_n^*/f_s^* for different M^* and ζ_s: ——, $f_n/f_s^* = f_n^*/f_s^*$; ---, equation (19), $M^* = 1$; – – –, equation (10), $M^* = 10$; ○, $M^* = 1$, $\zeta_s = 0{\cdot}003557$, 2-dof; +, $M^* = 10$, $\zeta_s = 0{\cdot}0003557$, 2-dof.

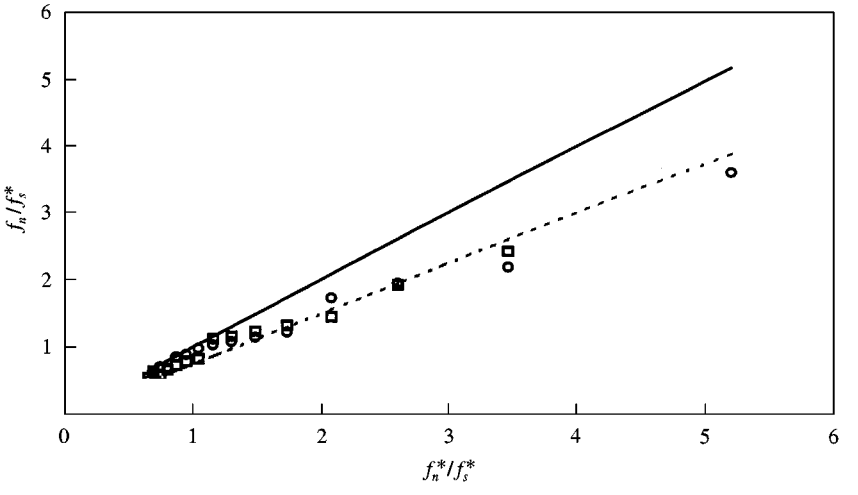

Figure 8. Variation of f_n with f_n^*/f_s^* for the same M^* and ζ_s: ——, $f_n/f_s^* = f_n^*/f_s^*$; ---, equation (19), $M^* = 1$; ○, $M^* = 1$, $\zeta_s = 0{\cdot}003557$, 2-dof; □, $M^* = 1$, $\zeta_s = 0{\cdot}003557$, 2-dof.

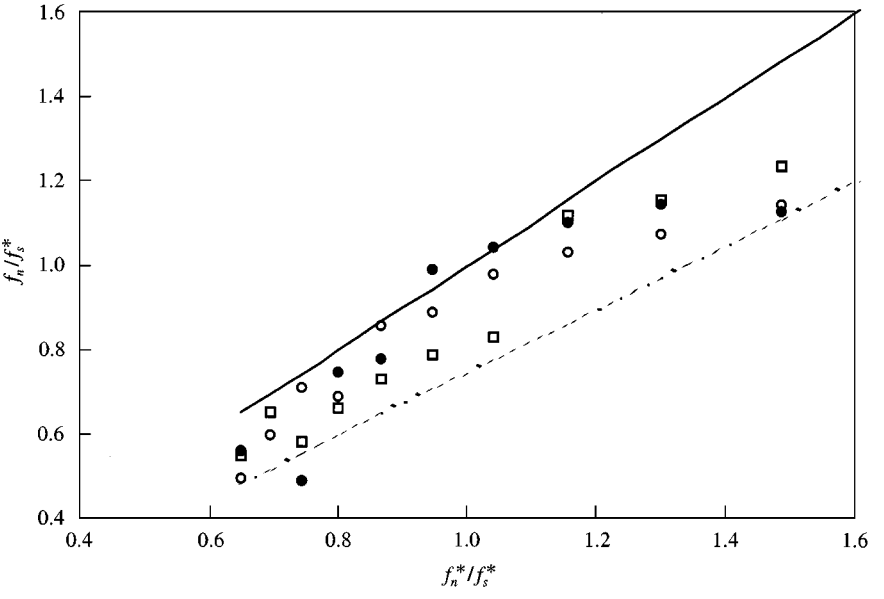

Figure 9. Comparison of the variation of f_n with f_n^*/f_s^* for the 1-dof and 2-dof systems: ——, $f_n/f_s^* = f_n^*/f_s^*$; ---, equation (19), $M^* = 1$; ○, $M^* = 1$, $\zeta_s = 0{\cdot}003557$, 2-dof; □, $M^* = 1$, $\zeta_s = 0{\cdot}03557$, 2-dof; ●, $M^* = 1$, $\zeta_s = 0{\cdot}003557$, 1-dof.

$f_n^*/\sqrt{1 + 4/\pi M^*}$. Therefore, it is not surprising to see that in the range of $f_n^*/f_s^* = 0{\cdot}87$ to $0{\cdot}65$, the value of f_n determined from ARMA is higher than that obtained from equation (19).

7. CONCLUSIONS

An identification technique based on the autoregressive moving-average (ARMA) method has been used to analyse the transverse displacement time histories obtained from a

numerical simulation of an elastic cylinder placed in a uniform cross-flow. This approach is used to investigate the effective damping ratio of the fluid-structure system. Since the structural damping ratio is very small compared to the fluid damping ratio, the effective damping ratio is essentially equal to the fluid damping ratio. It is found that there is a decrease in the fluid damping ratio in the region of synchronization, which indicates a low energy dissipation and a high energy transfer from the flow to the cylinder motion. Outside of the synchronization region, the fluid damping ratio increases as the amplitude of the vibration increases. It is further found that the mass ratio has a strong influence on fluid damping, i.e., the larger the mass ratio the smaller the fluid damping ratio. The credibility of these results is verified by an independent method, which depends on the analysis of the unsteady transverse force.

The method relies on the decomposition of the transverse fluid force into a drag (or out-of-phase) component and an inertia (or in-phase) component and their substitution into the structural dynamics equation for analysis. The damping ratios thus deduced are in agreement with the ARMA results, except in the region surrounding synchronization. In this region, the ARMA results are expected to be more reliable than those deduced from the force decomposition method. The reason is that the force decomposition method is essentially based on a one-frequency representation of the cylinder vibration, while the ARMA technique naturally accounts for multiple frequencies and thus can best model the cylinder response time histories near synchronization. Furthermore, the ARMA deduced damping ratios show a very similar trend to the experimental results obtained by Griffin and Koopmann (1977). This means that the ARMA technique is a good identification tool for flow-induced vibration problems.

ACKNOWLEDGEMENTS

The authors wish to acknowledge support given to them through the Central Research Grants (G-YW04 and G-V394) of The Hong Kong Polytechnic University and the Research Grants Council of the Government of the HKSAR under Grant No. PolyU 5159/97E.

References

Baban, F., So, R. M. C. & Otugen, M. V. 1989 Unsteady forces on circular cylinders in a cross-flow. *Experiments in Fluids* **7,** 293–302.

Baban, F. & So, R. M. C. 1991 Recirculating flow behind and unsteady forces on finite-span circular cylinders in a cross-flow. *Journal of Fluids and Structures* **5**, 185–206.

Batchelor, G. K. 1970 *An Introduction to Fluid Dynamics*, pp. 357. Cambridge: Cambridge University Press.

Blevins, R. D. 1994 *Flow-Induced Vibration.* Malabar, FL: Krieger Publishing Company.

Chen, S. S. & Jendrzejczyk, J. A. 1979 Dynamic response of a circular cylinder subjected to liquid cross flow. *ASME Journal of Pressure Vessel Technology* **101,** 106–112.

Griffin, O. M. & Koopmann, G. H. 1977 The vortex-excited lift and reaction forces on resonantly vibrating cylinders. *Journal of Sound and Vibration* **54,** 435–448.

Griffin, O. M., Skop, R. A. & Koopmann, G. H. 1973 The vortex-excited resonant vibrations of circular cylinders. *Journal of Sound and Vibration* **31,** 235–249.

Iyengar, R. N. 1988 Higher order linearization in non-linear random vibration. *International Journal of Non-Linear Mechanics* **23,** 385–391.

Jadic, I., So, R. M. C. & Mignolet, M. P. 1998 Analysis of fluid–structure interactions using a time marching technique. *Journal of Fluids and Structures* **12,** 631–654.

Juang, J. N. & Pappa, R. S. 1985 An eigensystem realization algorithm for modal parameter identification and model reduction. *Journal of Guidance, Control and Dynamics* **8,** 620–627.

Mignolet, M. P. Red-Horse, J. R. & Lin, C. C. 1993 A multistage ARMAX identification of structures. *Proceedings of the* 34*th Structures, Structural Dynamics, and Materials Conference, AIAA/ASME*, pp. 3366–3374. La Jolla, CA,U.S.A.

MIGNOLET, M. P. & RED-HORSE, J. R. 1994 ARMAX identification of vibrating structures: model and model order estimation. *Proceedings of the 35th Structures, Structural Dynamics, and Materials Conference, AIAA/ASME*, pp. 1628–1637. Hilton Head, SC, U.S.A.
NEWMAN, D. J. & KARNIADAKIS G. E. 1997 A direct numerical simulation study of flow past a freely vibrating cable. *Journal of Fluid Mechanics* **344,** 95–136.
RED-HORSE, J. R., ALVIN, K. F., MIGNOLET, M. P. & ROBERTSON, A. N. 1996 An investigation of three major time series data analysis techniques. *Proceedings of the 14th International Modal Analysis Conference*, pp. 1600–1607, Dearborn, MI.
SARPKAYA, T. 1979 Vortex-induced oscillations. *Journal of Applied Mechanics* **46,** 241–258.
SARPKAYA, T. & ISAACSON, M. 1981 *Mechanics of Wave Forces on Offshore Structures*. New York: Van Nostrand Reinhold.
SIN, V. K. & SO, R. M. C. 1987 Local force measurements on finite-span cylinders in a cross-flow. *ASME Journal of Fluids Engineering* **109,** 136–143.
SKOP, R. A. & BALASUBRAMMANIAN, S. 1997 A new twist on an old model for vortex-excited vibrations. *Journal of Fluids and Structures* **11,** 395–412.
SLAOUTI, A. & STANSBY, P. K. 1994 Forced oscillation and dynamics response of a cylinder in a current investigation by the vortex method. *Proceedings BOSS* 94, pp. 645–654. MIT Cambridge, MA, U.S.A.
SO, R. M. C., JADIC, I. & MIGNOLET, M. P. 1999 Fluid–structure resonance produced by oncoming alternating vortices. *Journal of Fluids and Structures* **13,** 519–548.
WOOD, K. N. & PARKINSON, G. V. 1977 A hysteresis problem in vortex-induced oscillation. *Proceedings of the sixth Canadian Congress of Applied Mechanics* (*CANCAM*), pp. 697–698. Vancouver, B.C., Canada.
ZHOU, C. Y. 1994 Effects of combination motion on cylinders in waves and current. Ph.D. Thesis, Imperial College, University of London, U.K.
ZHOU, C. Y., SO, R. M. C. & LAM, K. 1999 Vortex-induced vibrations of elastic circular cylinders. *Journal of Fluids and Structures* **13,** 165–189.

APPENDIX: NOMENCLATURE

a_y	cylinder acceleration along the y direction
C_a	added mass coefficient
C_D	mean drag coefficient
C_{dl}	lift drag coefficient
C_{ml}	lift inertia coeffcient
D	diameter of cylinder per unit length
F_x	x-component of induced force vector
F_y	y-component of induced force vector
f_n	natural frequency of fluid–cylinder system in Hz
f_n^*	natural frequency of cylinder only in Hz
f_s	vortex shedding frequency of vibrating cylinder in Hz
f_s^*	vortex shedding frequency of stationary cylinder in Hz
m	mass of cylinder per unit length
$M^* = m/\rho D^2$	ratio of cylinder mass over displaced fluid mass
$\mathrm{Re} = U_\infty D/\nu$	Reynolds number
$\mathrm{St} = f_s D/U_\infty$	Strouhal number of vibrating cylinder
$\mathrm{St}^* = f_s^* D/U_\infty$	Strouhal number of stationary cylinder
t	dimensional time
U_∞	free stream velocity
$V_r = U_\infty/f_n^* D$	reduced velocity
$V(t)$	instantaneous velocity
$V_{\max}$	amplitude of the instantaneous velocity
x	streamwise coordinate
X	x-component of cylinder displacement
y	transverse coordinate
Y	y-component of cylinder displacement

$Y_{\max}$	amplitude of the y displacement
ζ_e	effective damping ratio
ζ_f	fluid damping ratio
ζ_s	structural damping ratio
ζ_{ex}	effective damping ratio deduced from x-direction signal
ζ_{ey}	effective damping ratio deduced from y-direction signal
ζ_{fx}	fluid damping ratio deduced from x-direction signal
ζ_{fy}	fluid damping ratio deduced from y-direction signal
ν	fluid kinematic viscosity
ρ	fluid density
$\tau = tU_\infty/D$	non-dimensional time
$\omega_n = 2\pi f_n$	angular natural frequency of fluid-cylinder system
$\omega_s = 2\pi f_s$	angular frequency of vortex shedding